Robust Transfer of Optical Frequency over 500 km Fiber Link with Instability of 10^{-21}

Qian Zhou(周茜)[1,2,3,4], Xiang Zhang(张翔)[1,3*], Qi Zang(臧琦)[1,3], Mengfan Wu(吴梦凡)[1,3], Dan Wang(王丹)[1,2,3], Jie Liu(刘杰)[1,3], Ruifang Dong(董瑞芳)[1,2,3*], Tao Liu(刘涛)[1,2,3,4*], and Shougang Zhang(张首刚)[1,2,3]

[1]*National Time Service Center, Chinese Academy of Sciences, Xi'an 710600, China*
[2]*University of Chinese Academy of Sciences, Beijing 100049, China*
[3]*Key Laboratory of Time and Frequency Standards, Chinese Academy of Sciences, Xi'an 710600, China*
[4]*Hefei National Laboratory, Hefei 230088, China*

(Received 15 April 2024; accepted manuscript online 25 July 2024)

Our primary objective is to mitigate the adverse effects of temperature fluctuations on the optical frequency transmission system by reducing the length of the interferometer. Following optimization, the phase-temperature coefficient of the optical system is reduced to approximately 1.35 fs/K. By applying a sophisticated temperature control to the remained "out-of-loop" optics fiber, the noise floor of the system has been effectively lowered to 10^{-21} level. Based on this performance-enhanced transfer system, we demonstrate coherent transmission of optical frequency through 500-km spooled fiber link. After being actively compensated, the transfer instability of 4.5×10^{-16} at the averaging time of 1 s and 5.6×10^{-21} at 10000 s is demonstrated. The frequency uncertainty of received light at remote site relative to that of the origin light at local site is achieved to be 1.15×10^{-19}. This enhanced system configuration is particularly well suited for future long-distance frequency transmission and comparison of the most advanced optical clock signals.

DOI: 10.1088/0256-307X/41/8/084202

So far, trapped ion and neutral lattice optical clocks have achieved remarkable performance, showing a fractional uncertainty and instabilities at the order of 10^{-18} in various laboratories worldwide.[1–4] Conventional methods reliant on satellite-based technologies are no longer sufficient to attain the high-precision accuracy required for long-distance transmission and comparison of these optical clocks.[5,6] Consequently, a pressing challenge emerges: how to transmit and compare frequency signals generated by optical clocks over extended distances with minimal perturbation.

Optical fibers offer a promising transfer solution for these high-precision frequency signals without degrading their performance, provided that compensation mechanisms address signal attenuation and phase fluctuations induced by acoustic and thermal perturbations within the fiber link.[7–9] Numerous research groups across the globe have demonstrated the capacity to transfer and compare high-precision time and frequency signals using fiber-based frequency transfer techniques.[10–13] Given the growing significance of exploiting the inherent clock instability in many research fields, such as time and frequency metrology,[14] radio astronomy,[15,16] gravitational-wave detection,[17] and testing of fundamental physics,[18–20] development of highly stable fiber-based optical frequency transfer systems becomes increasingly crucial.

In recent years, diverse optical frequency transfer methodologies have undergone investigation, including the active noise compensation (ANC) method,[21] passive noise compensation (PNC) method,[22,23] and two-way comparison method.[24,25] The above-mentioned schemes are essentially based on all-fiber Michelson interferometers to detect and suppress fiber-induced optical phase noise arising from environment changes. Unfortunately, the inherent interferometer noise resulting from phase fluctuations of interferometer system's reference arms and the "out-of-loop" fibers in the measurement unit could not be effectively compensated. The non-suppressed interferometer noise will set a limitation in the long-term transfer instability of 10^{-20} level.[26] In order to remove the above-mentioned transfer limitations and improve performance of the system, a compact design of free-space interferometer is investigated and demonstrated, which can effectively improve the systemic uncertainty and instabilities because the thermo-optic coefficient of the free-space optics components is approximately three orders of magnitude lower than the optic fiber,[27] but the system performance is easily affected by the atmospheric turbulence and mechanical movement.[28] Another feasible solution is to build an optical frequency transfer system with planar lightwave circuits (PLCs), which exhibits an unprecedentedly low transmission instability noise floor of 1×10^{-21} at 5000 s averaging time.[30] However, its high cost and immature technology for some active phase-compensation

*Corresponding authors. Email: zhangxiang@ntsc.ac.cn; taoliu@ntsc.ac.cn; dongruifang@ntsc.ac.cn
© 2024 Chinese Physical Society and IOP Publishing Ltd

devices make it impossible to be widely used at present. Among all the existing schemes, the simplest one is to reduce the interference noise by precisely match the optical length while minimizing the fiber splicing distance and apply a precise temperature control for these out-of-loop optic fibers. Thus, an all-fiber optical frequency transfer system with low phase-temperature coefficient could be employed.

In this Letter, we concentrate on the minimization of interferometer noise in our high-precision optical frequency transfer system by substantially reducing the asymmetric portion of the optical path and implementing effective temperature control. After optimization, a lower phase-temperature coefficient of 1.35 fs/K for the frequency transfer system is demonstrated, with the transfer instability noise floor reaching 10^{-21} level. We present empirical evidence of the system's performance over a 500 km spooled fiber link, which achieves a fractional frequency instability of 4.5×10^{-16} at the integration time of 1 s and scales down to 5.6×10^{-21} at the integration time of 10000 s in terms of modified Allan deviation.

The detailed experimental setup of optical frequency transfer with ANC technology is shown in Fig. 1. The ultrastable optical frequency signal operated with a 1 Hz line width at central wavelength of 1550.12 nm, which was provided by a commercial fiber laser (NKT E15), and its frequency was locked to a Fabry–Pérot (FP) cavity with the Pound–Drever–Hall (PDH) technique.[31] Similar to our previous experimental setup demonstrated in Ref. [12], the optical frequency transfer system consists of a local and a remote site. In local site, the ultrastable laser is split into two parts with a 99/1 optical coupler (OC1). The small portion serves as a reference signal to detect the residual phase noise of retrieved optical signal at remote site, while the large portion of laser was used to transmitted. The transmitted light is divided into two parts by OC2. One part is directly reflected to the photo detector (PD1) by a Faraday mirror (FM1) as a reference signal, while the other part passes through an acousto-optic modulator (AOM1) operating at driving frequency of 110 MHz and is transmitted to the remote site through the single-mode fiber. In remote site, the transmitted light passes through the AOM2 and reflected most part to the PD1 of local site by FM2. The AOM2 gives a frequency shift of 50 MHz to discriminate the return signal from the stray reflections by the fiber link. In the ideal case, the out-loop phase noise can be perfectly compensated by canceling the in-loop phase noise detected by PD1. The resulting beating signal of 320 MHz between the round-trip signal and reference signal was detected by PD1, which carried the phase noise information of a fiber link. To compensate the optical loss of about 100 dB induced by 500 km fiber link, six bi-directional erbium-doped fiber amplifiers were arranged along the link. To mitigate nonlinear effects in the fiber, the gain of each amplifier is limited to 16 dB. In the measurement unit, the obtained beating signal of 160 MHz between retrieved light at the remote site and reference light is used to evaluate the transfer performance.

In this experiment, the optical units of the local site and the remote site are both placed in an aluminum box. The out-of-loop fibers are placed on aluminum sheets at the bottom of the box, with their temperature being controlled with a Peltier element.

Following the principle as described in Refs. [30,32], the phase fluctuation $\Delta\varphi_{\rm OOL}$ of the out-of-loop fiber in our case can be expressed as

$$\Delta\varphi_{\rm OOL}=\Delta\varphi_{\rm AB}+2\Delta\varphi_{\rm BC}+\Delta\varphi_{\rm EF'}-\Delta\varphi_{\rm EF}. \tag{1}$$

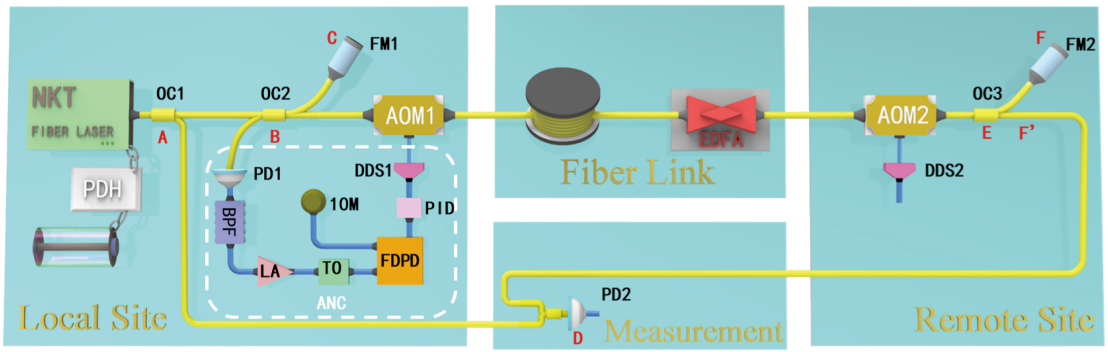

Fig. 1. Schematic diagram of the optical frequency transfer system. OC: optical coupler; FM: Faraday mirror; PD: photodetector; AOM: acousto-optic modulator; RF: radio frequency; FDPD: a programmable digital frequency division phase discriminator; EDFA: erbium-doped fiber amplifier. DDS: direct digital synthesis; BPF: band-pass filter; LA: logarithmic amplifier; TO: tracking oscillator. The point F′ is for remote user.

Here, $\Delta\varphi_{ij}$ represents the phase fluctuation introduced by the fiber segment from point i to point j, and the symmetry of the transmission path is assumed, $\Delta\varphi_{ij}=\Delta\varphi_{ji}$. In the measurement site, the fiber segments of AD and F′D have the same length for eliminating the asymmetry phase noise in the measurement process. Considering the fiber segments of AB, BC, EF and EF′ shown in Fig. 1, the equivalent length of the out-of-loop fiber can be expressed as

$$L_{\rm e}=L_{\rm AB}+2L_{\rm BC}+L_{\rm EF'}-L_{\rm EF}. \tag{2}$$

For achieving a high-performance optical frequency trans-

mission system, it is necessary to minimize the additional phase contribution. The fiber lengths of segments, i.e., L_{AB}, L_{BC}, L_{AD}, and $L_{\mathrm{F'D}}$, are reduced to about 10 cm, which is the permissible limit of the fiber fusion splicer. The point F′ is for remote user and the $L_{\mathrm{EF'}}$ is 5 cm, while the L_{EF} is controlled at about 35 cm.

The interferometer noise is mainly caused by the effect of temperature fluctuations on out-of-loop fibers. The phase variation induced by the interferometer noise can be elaborately expressed as a function of the temperature variation:

$$\delta\varphi(z,\,t) = \omega\frac{nL}{c}(\alpha+\xi)\delta T(z,\,t), \tag{3}$$

where ω is the optical carrier angular frequency at 193 THz, the fiber refraction index n is equal to 1.468, c is the speed of light in vacuum, and $\alpha = \frac{1}{L}\frac{\partial L}{\partial T} \sim 0.55\times10^{-6}\,\mathrm{K}^{-1}$ is the fiber linear expansion coefficient for silica, $\xi = \frac{1}{n}\frac{\partial n}{\partial T} \sim 7\times10^{-6}\,\mathrm{K}^{-1}$ is the therm-optic coefficient, δT is the variation of the temperature. Thus, when one considers that the influence of temperature to fiber section is well distributed, the total thermal phase variation can be simply expressed as

$$\delta\varphi(t) = \omega\gamma L_{\mathrm{e}}\delta T(t), \tag{4}$$

where $\gamma = 37\,\mathrm{fs\cdot K^{-1}\cdot m^{-1}}$ represents phase-temperature coefficient per unit length for the SMF-28 fiber specifications, L_{e} is the equivalent length of out-of-loop fibers. The systemic phase-temperature coefficient γL_{e}, characterizing the relevant time error (phase error) of the transfer system, can be expressed as

$$\gamma L_{\mathrm{e}} = \partial\varphi(t)/\partial T(t). \tag{5}$$

According to Eq. (5), if the temperature variation and corresponding phase change are obtained, we can make an approximate estimation of the systemic phase-temperature coefficient. The temperature measurements were taken using a digital multi-meter (Pico TC-08) with a 1 s averaging time. The phase data was calculated using frequency data measured by a K&K frequency counter with a 1 s gate time. To measure the phase-temperature coefficient of the system, the aluminum box was placed in a temperature-adjustable box, and the temperature controller was turned off. The experimental results are shown in Fig. 2, in a time period of approximately 800 s where the change of phase data and temperature data overlapped. The data demonstrates that a temperature change of approximately 1.5 K corresponds to a time error change of about 2 fs. Based on the measurement results, the phase-temperature coefficient of the system is approximately 1.35 fs/K. On top of this, a sophisticated temperature controller is employed to the out-of-loop fibers, the temperature fluctuations of laboratory environment and out-of-loop fibers are simultaneously recorded by the digital multi-meter, as shown in Fig. 3. The peak-to-peak temperature variation around out-of-loop fibers be effectively reduced to 20 mK in the case of a temperature-adjustable box temperature change of about 10 K.

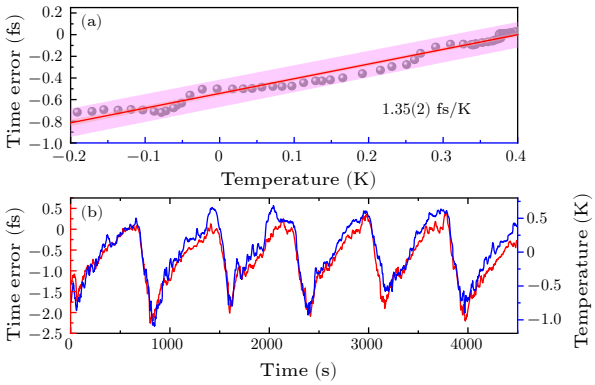

Fig. 2. Relationship between temperature and induced systemic time error. Temperature variation around the interferometer setup (red trace) and the induced time error of the tested signal (blue trace) expressed in fs as a function of time. The phase-temperature coefficient of the system is approximately 1.35 fs/K.

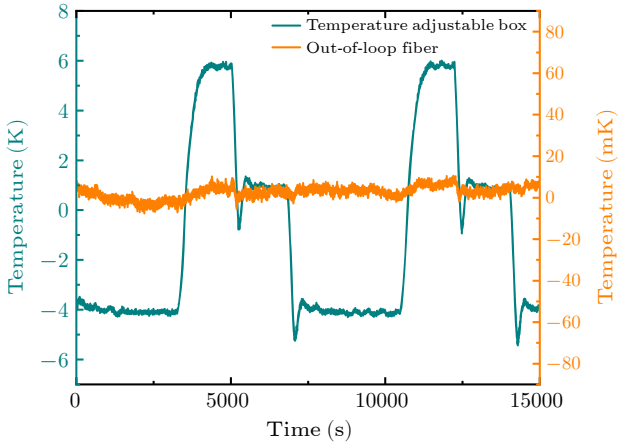

Fig. 3. Recording temperature variation of the laboratory environment (green curve) and out-of-loop fibers (orange curve). With the implementation of temperature controller, the peak-to-peak temperature variation is effectively reduced from 10 K to 20 mK.

For measuring the system noise floor and the transfer instability of 500 km fiber-based optical frequency transmission, the aluminum box was placed in the wooden box for passive temperature isolation. To measure the noise floor, a tunable optical fiber attenuator of about 1 m was used to connect the local site and remote site. The temperature control accuracy can be maintained at approximately 20 mK. The optical system was tested before and after optimization when the circuit system was closed loop. To characterize the performance of the optical system, we measure the frequency instability of the transferred light relative to the outgoing signal light, where the frequency data was obtained from the K&K frequency counter in Λ type with a gate time of 1 s.

Figure 4(a) shows the frequency domain characterization of the systemic system floor in terms of phase noise power spectrum density (PSD) under the free-running and stabilized condition. The free-running phase noise PSD is dominated by $S_\varphi \sim 10^{-3}\cdot f^{-6}\,\mathrm{rad^2/Hz}$ below a Fourier frequency of 5 Hz. The phase noise PSD also exists some

bumps at frequencies of 40 Hz and 50 Hz, and we attributed it to the vibrations from the equipment operation in the laboratory. Once the system is under the phase-compensated condition, the phase noise PSD is dominated by $S_\varphi \sim 10^{-6} \cdot f^{-1}\,\mathrm{rad}^2/\mathrm{Hz}$, a noise suppression ratio of 30 dB at Fourier frequency of 1 Hz is obtained. Figure 4(b) illustrates the time domain characterization of the systemic system floor in terms of the fractional frequency instability under a stable condition. The measurement results are shown by using modified Allan deviation (Mod-ADEV). We can clearly see that the fractional frequency instability achieves 1×10^{-17} at integration time of 1 s and scales down to 2.7×10^{-21} at integration time of 8000 s. The results show that the system achieves a better performance of long-term instability and is suitable for the further transfer and comparison of these state-of-the-art optical clock signals.

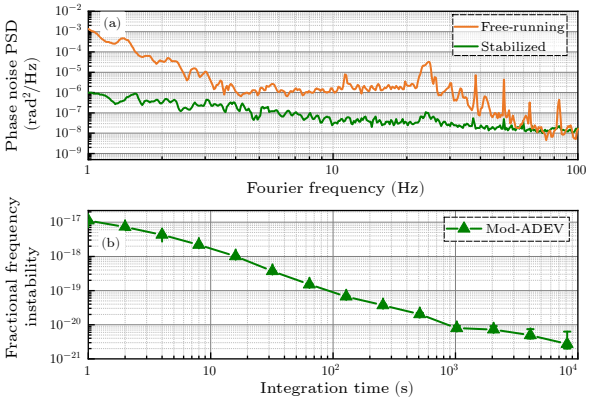

Fig. 4. Measurement results of systemic noise floor: (a) measured phase noise PSDs under the free-running condition (orange curve) and the stabilized condition (green curve) by using the short-cutting method, (b) the fractional frequency instability of the transfer system under the stabilized condition (green triangle).

Figure 5 illustrates the characteristic of 500 km fiber link phase noise PSDs in the free-running case and the stabilized case. The phase noise was obtained from the frequency data taken with a K&K counter at a gate time of 1 ms. The free-running phase-noise PSD of this employed 500 km fiber link approximately follows a power-law relationship, $S_{\mathrm{free}} \sim h_0 \cdot f^{-2}\,\mathrm{rad}^2/\mathrm{Hz}$, indicating that the white frequency noise is dominant under the noise uncompensated condition. The coefficient h_0 varies with fiber length and exhibits noise information for the fiber link, and is up to approximately 3000 in this study. After actively compensating the fiber link induced phase fluctuation, the noise reduction in phase-noise PSD domain at 1 Hz is approximately 40 dB. The residual phase-noise PSD, denoted as $S_{\mathrm{r}}(f)$, demonstrates a dependence with the lower Fourier frequency of $h_1 f^0$, indicating that the remaining noise is primarily determined by the white phase noise, $h_1 \sim 0.8$. In the stabilized case, a servo bump at around 80 Hz is visible as shown in Fig. 5, which is caused by the time delay τ along fiber link and is closed to the theoretical servo bandwidth $(1/4\tau)$ of 100 Hz. For the 500 km fiber, the induced time delay $\tau = nL/c \sim 2.5$ ms, where $n = 1.468$ is the refractive index of fiber link. The one-way transmitted stabilized signal will still be affected by unsuppressed noise, even if the noise of the round-trip light is perfectly eliminated. Taking fiber delay τ into account, the theoretical compensation limitation of phase noise PSD $S_{\mathrm{D}}(f)$ can be calculated by [33]

$$S_{\mathrm{D}}(f) = \frac{1}{3}(2\pi f\tau)^2 S_{\mathrm{free}}. \tag{6}$$

The numerical result is also shown in Fig. 5, and we can see that the residual phase-noise PSD $S_{\mathrm{r}}(f)$ approximately coincides with the theoretical compensation limitation.

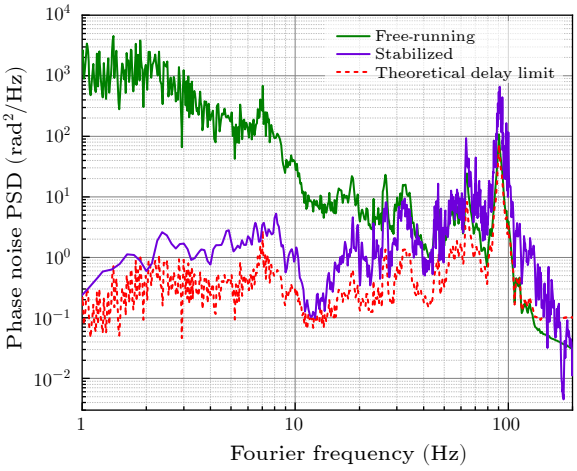

Fig. 5. Measured phase noise PSDs via the 500 km spooled fiber link in free running (green solid line) and stabilized case (purple solid line). The delay-induced theoretical compensated limitation (red dashed line) is also shown.

The corresponding plots of fractional frequency instability via the 500 km spooled fiber link are given in Fig. 6. The frequency data were continuously measured by K&K frequency counter in Π type and Λ type at 1 s gate time. The Λ type of frequency counter (phase averaging mode) is similar to applying a sinc-shaped low-pass filter to the phase fluctuations, which effectively reduces approximately two orders of the instability at 1 s than the Π type (full-bandwidth mode).[34,35] In the free-running case, the fractional frequency instability is 8.3×10^{-14} at 1 s integration time and fluctuates around the 10^{-14} level. With the implementation of the fiber noise cancelation, optical frequency transfer achieves a fractional frequency instability of 3.1×10^{-14} at an integration time of 1 s in terms of Mod-ADEV, and falls to 1.7×10^{-20} with a slope of $\tau^{-3/2}$ at averaging times of up to 10000 s, showing the characteristic response of the white phase noise under the stabilized 500 km fiber condition. In the Λ-type counter, the fractional frequency instability achieve 4.5×10^{-16} at 1 s and scales down to 5.6×10^{-21} at integration time of 10000 s. This result demonstrates the reliability of the transfer system and proves that the system can be used for the further transfer and comparison of the most advanced clock signal.

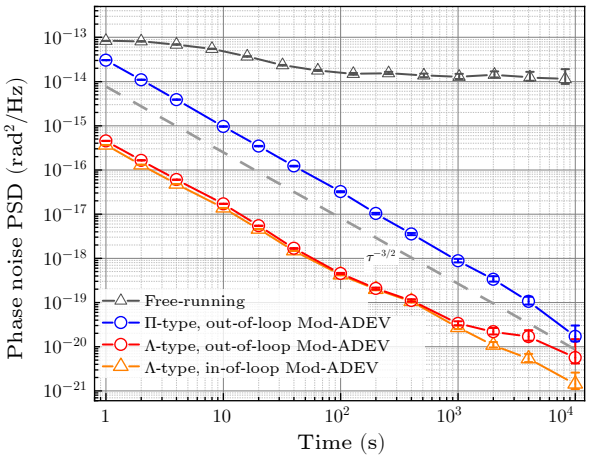

Fig. 6. Fractional frequency instability in terms of Mod-ADEV via the 500 km spooled fiber link in the free-running case (black triangles) and stabilized case (blue circles for Π type, red circles for Λ type). The in-loop frequency data (range triangles) were recorded per second operating at the Λ type.

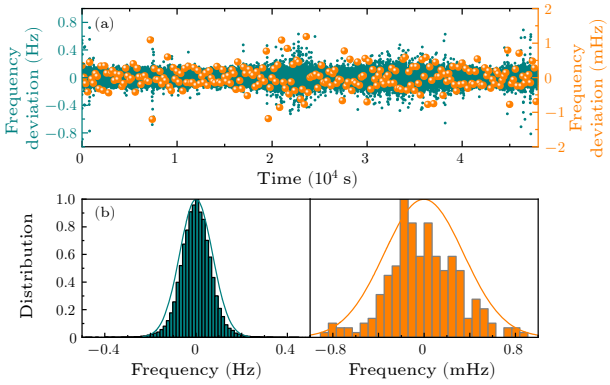

Fig. 7. (a) Recorded 47911 data taken from the end-to-end beat signal for the stabilized 500 km spooled fiber link with a dead-time free Λ-mode frequency counters with a 1 s gate time (dark cyan points, left axis). The unweighted arithmetic means for all cycle-slip free 200-s long segments were calculated, resulting in 239 data (orange points, right frequency axis). (b) Histograms and Gaussian fit for the recorded frequency values (dark cyan color) and above-mentioned 239 arithmetic mean values (orange color).

Besides the time domain characterization, the accuracy is further assessed through the analysis of end-to-end beat note frequencies. The frequency deviation of the transferred signal, subsequent to the active stabilization of a 500 km fiber link, is illustrated in Fig. 7(a). This data is continuously acquired by employing a Λ-type frequency counter with a 1 s gate time, yielding a total of 47911 data (depicted as dark cyan points on the left axis). By averaging the frequency data every cycle slip free 200 s, resulting in 239 data as shown in Fig. 7(a). Figure 7(b) illustrates the histograms and Gaussian fit for the recorded frequencies and above-mentioned 239 arithmetic mean values, respectively. According to the Gaussian fit, the arithmetic mean of the total 239 data is 0.41 μHz (2.11×10^{-21}) in the standard deviation of 0.35 mHz (1.80×10^{-18}). The statistical fractional frequency uncertainty is 22.6 μHz (1.15×10^{-19}) and the retrieved light at remote site has no frequency deviation relative to the reference light within this uncertainty.

In summary, we aim to mitigate the impact of temperature on the optical frequency transmission system by decreasing the length of the interferometer. The phase-temperature coefficient of the optical system is approximately 1.35 fs/K after optimization. The noise floor of the system reaches the level of 10^{-21}. This system is more suitable for long-distance optical frequency transmission due to its low noise floor, which ensures that the long-term stability of the transmission will not be hindered by interferometer noise. We demonstrates the performance of the optical system, achieving an instability of 4.5×10^{-21} at an averaging time of 10000 s over a 500 km spooled fiber. The results show that this study establishes a foundation for the investigation of optical comparison networks.

Acknowledgment. This work was supported by the National Natural Science Foundation of China (Grant Nos. 12303076 and 12303077).

References

[1] Chou C W, Hume D B, Koelemeij J C J, Wineland D J, and Rosenband T 2010 *Phys. Rev. Lett.* **104** 070802

[2] Huntemann N, Sanner C, Lipphardt B, Tamm C, and Peik E 2016 *Phys. Rev. Lett.* **116** 063001

[3] Origlia S, Pramod M S, Schiller S, Singh Y, Bongs K, Schwarz R, Al-Masoudi A, Dörscher S, Herbers S, Häfner S, Sterr U, and Lisdat C 2018 *Phys. Rev. A* **98** 053443

[4] Hinkley N, Sherman J A, Phillips N B, Schioppo M, Lemke N D, Beloy K, Pizzocaro M, Oates C W, and Ludlow A D 2013 *Science* **341** 1215

[5] Fujieda M, Gotoh T, Nakagawa F, Tabuchi R, Aida M, and Amagai J 2012 *IEEE Trans. Ultrason. Ferroelectr. Freq. Control* **59** 2625

[6] Tseng W H, Lin S Y, Feng K M, Fujieda M, and Maeno H 2010 *IEEE Trans. Ultrason. Ferroelectr. Freq. Control* **57** 161

[7] Delva P, Lodewyck J, Bilicki S, Bookjans E, Vallet G, Le Targat R, Pottie P E, Guerlin C, Meynadier F, Le Poncin-Lafitte C, Lopez O, Amy-Klein A, Lee W K, Quintin N, Lisdat C, Al-Masoudi A, Dörscher S, Grebing C, Grosche G, Kuhl A, Raupach S, Sterr U, Hill I R, Hobson R, Bowden W, Kronjäger J, Marra G, Rolland A, Baynes F N, Margolis H S, and Gill P 2017 *Phys. Rev. Lett.* **118** 221102

[8] Foreman S M, Holman K W, Hudson D D, Jones D J, and Ye J 2007 *Rev. Sci. Instrum.* **78** 021101

[9] Cantin E, Tønnes M, Le Targat R, Amy-Klein A, Lopez O, and Pottie P E 2021 *New J. Phys.* **23** 053027

[10] Droste S, Ozimek F, Udem T, Predehl K, Hänsch T W, Schnatz H, Grosche G, and Holzwarth R 2013 *Phys. Rev. Lett.* **111** 110801

[11] Hu L, Tian X, Wang L, Wu G, and Chen J 2020 *J. Lightw. Technol.* **38** 5916

[12] Zhang X, Deng X, Zang Q, Jiao D, Gao J, Wang D, Zhou Q, Liu J, Xu G, Dong R, Liu T, and Zhang S 2022 *Chin. Phys. Lett.* **39** 044201

[13] Koke S, Kuhl A, Waterholter T, Raupach S M F, Lopez O, Cantin E, Quintin N, Amy-Klein A, Pottie P E, and Grosche G 2019 *New J. Phys.* **21** 123017

[14] Schioppo M, Kronjäger J, Silva A *et al.* 2022 *Nat. Commun.* **13** 212
[15] He Y, Baldwin K G, Orr B J *et al.* 2018 *Optica* **5** 138
[16] Clivati C, Ambrosini R, Artz T *et al.* 2017 *Sci. Rep.* **7** 40992
[17] Kolkowitz S, Pikovski I, Langellier N, Lukin M D, Walsworth R L, and Ye J 2016 *Phys. Rev. D* **94** 124043
[18] Roberts B M, Delva P, Al-Masoudi A, Amy-Klein A *et al.* 2020 *New J. Phys.* **22** 093010
[19] Filzinger M, Dörscher S, Lange R, Klose J, Steinel M, Benkler E, Peik E, Lisdat C, Huntemann N 2023 *Phys. Rev. Lett.* **130** 253001
[20] Wcisło P, Ablewski P, Beloy K *et al.* 2018 *Sci. Adv.* **4** eaau4869
[21] Ma L S, Jungner P, Ye J, and Hall J L 1994 *Opt. Lett.* **19** 1777
[22] Hu L, Tian X, Wu G, and Chen J 2020 *Opt. Lett.* **45** 4308
[23] Zhang X, Hu L, Deng X, Zang Q, Jiao D, Gao J, Wang D, Zhou Q, Liu J, Xu G, Liu T, Dong R, and Zhang S 2023 *Opt. Laser Technol.* **157** 108738
[24] Bercy A, Stefani F, Lopez O *et al.* 2014 *Phys. Rev. A* **90** 061802
[25] Calosso C E, Bertacco E, Calonico D, Clivati C, Costanzo G A, Frittelli M, Levi F, Mura A, and Godone A 2014 *Opt. Lett.* **39** 1177
[26] Coddington I, Swann W C, Lorini L *et al.* 2007 *Nat. Photon.* **1** 283
[27] Williams P A, Swann W C, and Newbury N R 2008 *J. Opt. Soc. Am. B* **25** 1284
[28] Jürss T, Grosche G, and Koke S 2023 *Photon. Res.* **11** 1113
[29]
[30] Akatsuka T, Goh T, Imai H *et al.* 2020 *Opt. Express* **28** 9186
[31] Jiao D, Gao J, Deng X, Xu G, Liu J, Liu T, Dong R, and Zhang S 2020 *Opt. Commun.* **463** 125460
[32] Grosche G 2014 *Opt. Lett.* **39** 2545
[33] Newbury N R, Williams P A, and Swann W C 2007 *Opt. Lett.* **32** 3056
[34] Dawkins S T, McFerran J J, and Luiten A N 2007 *IEEE Trans. Ultrason. Ferroelectr. Freq. Control* **54** 918
[35] Raupach S M F, Koczwara A, and Grosche G 2015 *Phys. Rev. A* **92** 021801